(Article begins on next page)

Fixed-point Processing for an IR Positioning System based on QADA Receivers

David Moltó, Álvaro Hernández, Elena Aparicio-Esteve, Jesús Ureña, Mª Carmen Pérez-Rubio

Electronics Department, University of Alcalá

Alcalá de Henares, Spain

david.molto@edu.uah.es; {alvaro.hernandez, elena.aparicio, jesus.urena, mcarmen.perezr}@uah.es

Abstract—Indoor optical positioning systems have increased in popularity in recent years because they can provide centimeter accuracy in three dimensions (3D) utilizing light-emitting diodes (LEDs) and photoreceptors. This work presents the design of a positioning system, which is based on a set of four photoreceptors functioning as beacons at known places for a single LED to be positioned. However, it might be extended to additional emitters with some medium access control. The associated processing is explained, as well as the basic assumptions to be addressed when approaching its hardware implementation, such as the preliminary partitioning of tasks between hardware and software, and the fixed-point representation of the processing to be implemented in hardware. The system has been validated by simulation in a $2 \times 2 \times 3.4$ m^3 volume, yielding mean absolute errors around 0.004 m for the X and Y axes, and around 0.01 m for the Z-axis, as well as lower standard deviations than 0.004 m for the X and Y axes and 0.01 m for the Z-axis.

Index Terms—Indoor optical positioning system, photoreceptors, fixed-point representation, FPGA.

I. INTRODUCTION

In recent years, global navigation satellite systems (GNSS) have been developed and widely used. However, in terms of indoor positioning, these systems have found significant limitations, such as low resolution and limited coverage. Other positioning solutions have emerged to replace GNSS in indoor contexts to solve these issues. Local positioning systems (LPS) give location information in the coverage area within a direct line-of-sight (LOS) between multiple transmitters and a receiver or between a transmitter and numerous receivers. According to the type of signal used, LPSs may be classified into: radio-frequency, magnetic, mechanical, acoustic, optical, etc. [1].

Due to their low cost, ease of integration into the work environment [2], and absence of health risk [3], LPS based on optical signals, visible light or infrared (IR), have begun to gain popularity. Both outdoor and indoor positioning is possible with these devices. Because of the significant impact that ambient light has on this sort of systems, most efforts are on indoor placements [4]. Although the transmitter in

indoor environments is commonly a light or an array of LEDs (Light Emitting Diode), we may distinguish between positioning systems based on image sensors and all those based on photoreceptors at the receiver. Cameras, such as those found in a typical mobile phone [5], or CMOS cameras [3] [6], are used in image sensor-based positioning systems. They do, however, need image processing methods, which slow down and complicate position calculation [7].

Photodiodes [8] [9], or an array of photodiodes [10] [11], are used in photoreceptor-based positioning systems; those generate a current used to estimate the receiver's position by using the appropriate positioning algorithm whether stimulated by light. These most notably include Quadrant Photodiode Angular Diversity Aperture (QADA) [10]. Multilateration, fingerprinting, or triangulation are the most popular positioning techniques in these instances, using time-of-flight measures (TOA, Times-of-Arrival; TDOA, Time-Difference-of-Arrival) [11], signal attenuation measurements (RSS, Received Signal Strength) [12] [13], or angle-of-arrival measurements (AOA, Angle-of-Arrival) [14]. Other strategies are also involved, such as proximity [15]. The main disadvantages of calculating time-of-flight measurements are the required synchronization and the speed of light, which allows 1 ns time estimate inaccuracies to result in a 30 cm position inaccuracy [16].

System-on-Chip (SoC) architectures based on FPGA (Field-Programmable Gate Arrays) devices, which allow the integration of hardware designs with general-purpose processors [17], are one of the choices for real-time implementation of processing and control algorithms and methods related to these LPSs. They enable high-speed signal processing, while including the processor's adaptability for communications or addressing specialized tasks that are not suitable for hardware implementation.

This work proposes and tests an indoor optical positioning system, based on using a LED as transmitter and QADA-type photoreceptor arrays as receivers. Triangulation is applied to estimate the transmitter's position, by using the angle-of-arrival (AOA) measurements between the transmitter and receivers. For that purpose, the positioning system architecture is analyzed, by evaluating various system parameters and their effects on the final performance; furthermore, a study of the

fixed-point representation is carried out, which will then be implemented in the configurable logic of a SoC architecture. In this way the main contributions of this work is the design and simulation of the entire positioning system, considering the fixed-point representation at the receiver's processing, and setting the guidelines for a future implementation in a SoC architecture. The rest of the manuscript is organized as follows: Section II describes the IR detector used and its associated signal processing; Section III details the fixed-point representation of the tasks to be implemented in the programmable logic; Section IV shows some preliminary simulated results; and finally, conclusions are discussed in Section V.

II. DESCRIPTION OF THE POSITIONING SYSTEM

Four circular QADA photoreceptors with a radius $r = 3.9$ mm are the IR signal receivers. These photoreceptors are covered with a square aperture of side $l = 2.75$ mm at a height of $h_{ap} = 2.6$ mm. This setting guarantees that the light beam always falls within the sensor's sensitive region, preventing border issues (i.e., non linearity in the calculations [18]). Although their axes are not aligned, the four receivers create a rhomboidal structure with a spacing of 5 cm between their centers, as shown in Fig. 1. The transmitter is a LED device that emits a BPSK-modulated signal, coded with a 1151-bit LS code, with a 127-bit interference-free window (IFW), derived from 512-bit Golay pairs [19]. These sequences are involved due to their suitable characteristics that guarantee a significant reduction of multiple access interference (MAI) [20]. This LS sequence is modulated with a square carrier of frequency 25kHz (to eliminate the effect of flickering with its consequent negative effects on health [21], a much higher carrier frequency than 200 Hz has been fixed), and one carrier period per bit. At reception, the incoming signal is acquired at a sampling rate of 250 kS/s, i.e., with an oversampling of 10.

Figure 2 shows the proposed design for the IR receiver, which consists of four processing units. The first block demodulates and correlates the input signals. The second block detects the maximum values of the correlation signals; the third stages estimates the central impact points of the light beams on the QADA receiver, based on the correlation maxima; and the fourth block calculates the IR emitter's position. The details of each part in the architecture are presented below.

A. Demodulation and Correlation

Each QADA photoreceptor is formed by four quadrant photodiodes, which, when an infrared beam impacts on them, generate an electrical current proportional to the illuminated area. Passing through a conditioning stage, these currents are converted into three signals per QADA: $r_{sum}[n]$ is the total sum of the four quadrants in the QADA; $r_{bt}[n]$ is the difference between the bottom and upper quadrants; and $r_{lr}[n]$ is the difference between the left and right quadrants. The block is divided into two stages, as shown in Fig. 3, one for the demodulation of the input signal
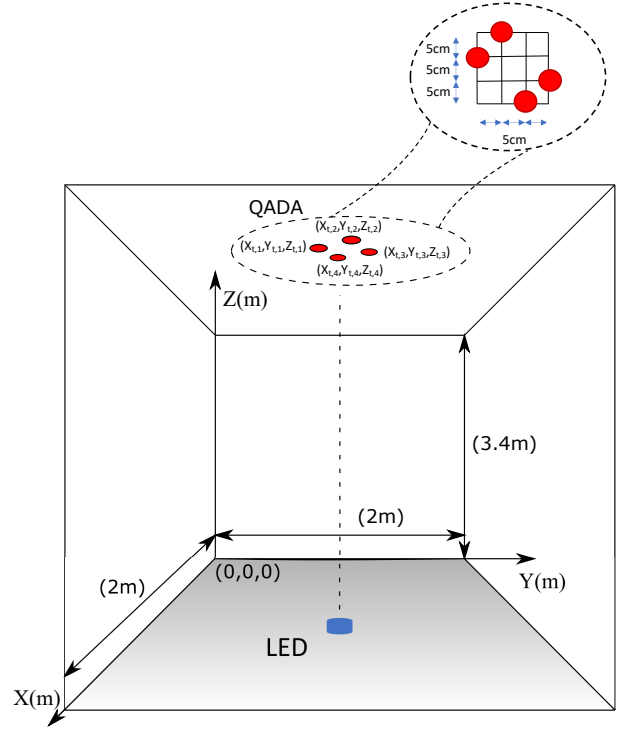

Fig. 1. Geometric distribution of the proposed system, deployed in the environment simulated for the later validation.
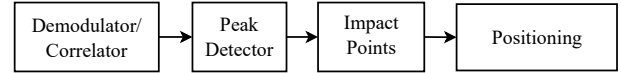

Fig. 2. General block diagram of the processing proposed for the IR detector.

$r[n]$ and the other for an efficient correlator, according to [19].

Since the signal processing at the receiver is repeated for the three input signals, $r_{sum}[n]$, $r_{bt}[n]$ and $r_{lr}[n]$, for clarity's sake, hereinafter the signal $r[n]$ represents indistinctly any of these three signals. The proposed demodulation has been simplified (1) due to the modulation symbol's features. Since this is a square signal with values $+1$ and -1, the solution is reduced to a difference equation in (2), which discards the multiplications and reduces the demodulation to a sum of the input sample $r[n]$, the input sample delayed $\beta/2$, $r[n - \beta/2]$, the input sample delayed β, $r[n - \beta]$, where the oversampling ratio $\beta = fs/fc$. This architecture is depicted in Fig. 4. It also requires a buffer with the last β samples. Using this architecture, the three input signals, $r_{sum}[n]$, $r_{bt}[n]$ and $r_{lr}[n]$, are demodulated.

$$d[n] = \sum_{k=0}^{(\beta/2)-1} r[n-k] - \sum_{k=\beta/2}^{\beta-1} r[n-k] \qquad (1)$$

$$d[n] = r[n] + 2 \cdot r\left[n - \frac{\beta}{2}\right] - r[n - \beta] + d[n-1] \qquad (2)$$

As depicted in Fig. 6, an efficient correlation scheme is applied here. It firstly consists in correlating the demodulated sequence $d[n]$ with the Golay pairs, S_0 and S_1, which
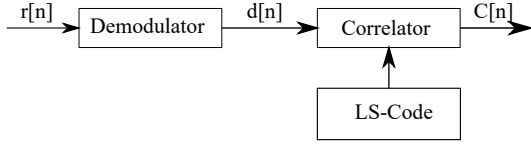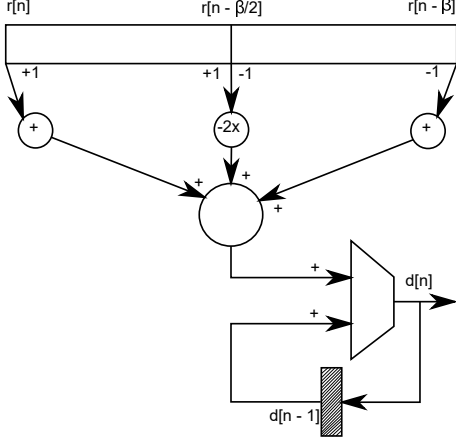
Fig. 3. Demodulator/Correlator diagram block

Fig. 4. Block diagram for the proposed simplified demodulator.

compose the LS code, by means of a correlator for sets of complementary sequences (CSS), generalized for Golay pairs (2-CSS) [22] [23]. Figure 5 describes this method, also known as 2-ESSC (Efficient Set of Sequences Correlator), which has two outputs that correspond to the simultaneous correlation of the input signal $d[n]$ with the two complementary sequences S_i in the set. Due to the oversampling in the LS sequences, the delay blocks Z^{-D_N} in the efficient correlator are scaled by $\beta = 10$.

Using a 2-ESSC correlator instead of a standard straightforward implementation allows the global number of operations to be reduced. In this general scheme, the correlation of the input signal with the M sequences of the set requires $M \cdot L$ multiplications and $M \cdot (L - 1)$ sums; however, the 2-ESSC only requires $\frac{M}{2} \cdot \log_2 L$ products and $M \cdot \log_2 L$ additions. Note that $M = 2$ represents the number of Golay sequences, $L = M^N$ represents the length of these sequences, and $N = 7$ is the size of the seed employed in the Golay pair generation [19].

An LS codes correlator is implemented starting from the efficient correlator for complementary sequences (see Fig. 6) [19], which can be expressed as (3, 4). This is an adaptation of the generic efficient correlator to LS sequences and has been named the efficient LS-codes correlator (ELSC), since it requires fewer operations than a direct correlator [19].

$$C[n] = \sum_{i=0}^{K/2-1} h_{k,i} z^{-(\frac{K}{2}-i-1) \cdot L_0}$$
$$\left[z^{-(\frac{K}{2} \cdot L_0 + W)} C_{R,S_{\pi_i},0}[n] + C_{R,S_{\pi_i},1}[n] \right] \quad (3)$$

$$C_{k+K/2}[n] = \sum_{i=0}^{K/2-1} h_{k,i} z^{-(\frac{K}{2}-i-1) \cdot L_0}$$
$$\left[z^{-(\frac{K}{2} \cdot L_0 + W)} C_{R,S_{\pi_i^*},0}[n] + C_{R,S_{\pi_i^*},1}[n] \right] \quad (4)$$

Where $C[n]$, with $0 \le k \le \frac{K}{2}$, denotes the correlation between the input signal $d[n]$ and the LS code; $h_{k,i} \in \{-1, 1\}$ denotes the Hadamard matrix elements employed in the generation of the Golay sequences; and $C_{R,S_{\pi_i},0}(z)$ and $C_{R,S_{\pi_i},1}(z)$ denote the correlations between the signal $d[n]$ and the sequences S_0 and S_1 in the set, respectively. The 2-ESSC efficient correlators performs the latter correlations, which decreases the total number of operations required in the final LS coding correlation, as detailed in [19]. As before, for clarity's sake, this architecture is actually used to correlate the three demodulated sequences, $d_{sum}[n]$, $d_{lr}[n]$ and $d_{bt}[n]$ obtained from the efficient demodulators explained above.

B. Detection of the Maximum Correlation Values

The correlation signal of the sum $C_{sum}[n]$ is used for the maximum detection since it has the largest amplitude of the three. The signal's absolute maximum, positive or negative, is used to determine the maximum values in the other two correlation signals at the same time instant. The highest value of the sum V_{sum} allows to normalize the maximum values from V_{lr} and V_{bt}, according to (5).

$$\hat{P}_x = \frac{V_{lr}}{V_{sum}}$$
$$\hat{P}_y = \frac{V_{bt}}{V_{sum}} \quad (5)$$

C. Central Impact Points Estimation

The central point of incidence (x_r, y_r) of the light beam from the IR emitter on the QADA receiver may be computed by using $\hat{P}_x$ and $\hat{P}_y$ ratios. Notice that the following additional intrinsic parameters to a pin-hole system affect the calculation of the light's center of incidence [18]: the optical center (x_c, y_c) is the center of the square aperture; the height h_{ap} at which the aperture is located (equivalent to the focal length); the aperture misalignment δ is defined as the rotation of the aperture about the photoreceptor axis; and the side of the square aperture l. With the optical center (x_c, y_c) and the focal length correction h_{ap}, the central point of incidence $\begin{bmatrix} x_{r,\lambda,c} \\ y_{r,\lambda,c} \end{bmatrix}$ can be set, according to (6), where λ is the ratio between the expected focal length h_{ap} and the actual focal length h'_{ap}: $\lambda = (\frac{h'_{ap}}{h_{ap}})$.

$$\begin{bmatrix} x_r \\ y_r \end{bmatrix} = \frac{-l}{2} \cdot \lambda \cdot \begin{bmatrix} P_x \\ P_y \end{bmatrix} \cdot \begin{bmatrix} x_c \\ y_c \end{bmatrix} \quad (6)$$
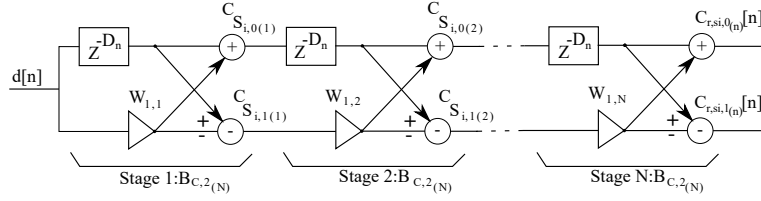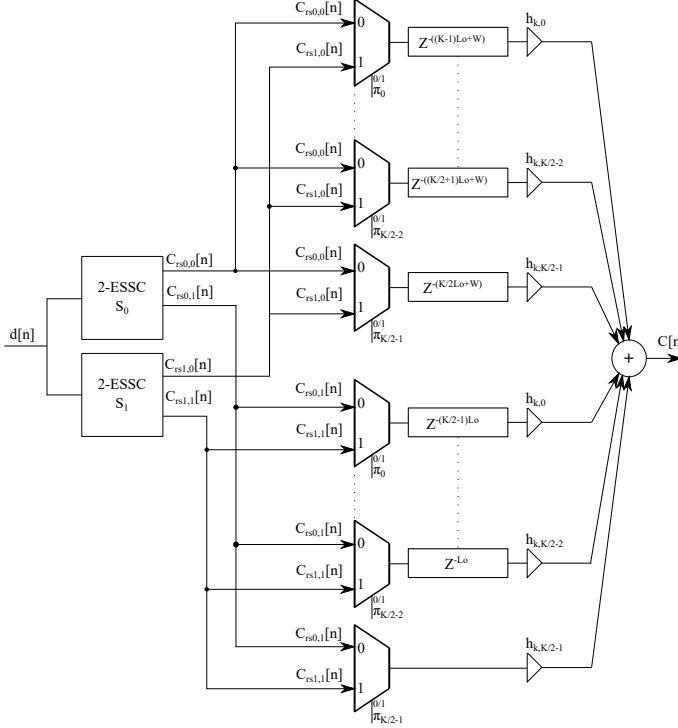
Fig. 5. 2-ECSS architecture.

Fig. 6. Block diagram of the the efficient LS-code correlator.

D. IR-Emitter Position Estimation

The last part of the proposed algorithm involves calculating the IR emitter's final position. The image points $(x_{r,i}, y_{r,i})$, the position $(x_{t,i}, y_{t,i}, z_{t,i})$ of the photoreceptors i, the aperture height h_{ap} (focal length) of the QADAs, and a previous estimate (or initialization) of the transmitter position are all used in the positioning algorithm. With these data, the positioning method applies a least-squares estimator (LSE) to obtain the IR emitter's location (x, y), so $(x, y) = (\mathbf{A}^T \cdot \mathbf{A})^{-1} \cdot \mathbf{A}^T \cdot \mathbf{b}$, according to (7).

$$\mathbf{A} = \begin{bmatrix} -y_{r,1} & x_{r,1} \\ -y_{r,2} & x_{r,2} \\ -y_{r,3} & x_{r,3} \\ -y_{r,4} & x_{r,4} \end{bmatrix} \quad \mathbf{b} = \begin{bmatrix} y_{t,1} \cdot x_{r,1} - x_{t,1} \cdot y_{r,1} \\ y_{t,2} \cdot x_{r,2} - x_{t,2} \cdot y_{r,2} \\ y_{t,3} \cdot x_{r,3} - x_{t,3} \cdot y_{r,3} \\ y_{t,4} \cdot x_{r,4} - x_{t,4} \cdot y_{r,4} \end{bmatrix} \quad (7)$$

Where $(x_{t,i}, y_{t,i}, z_{t,i})$ are the positions of the photoreceptors i. Following the estimation of the emitter's coordinates (x, y), the coordinate z is calculated by using trigonometric considerations, which include the distances d_i between the estimated transmitter position and the projection of each

QADA photoreceptor on the plane where the transmitter is positioned [18], as detailed in (8).

$$z = z_{t,i} - h_{ap} \cdot \left(1 + \sqrt{\frac{(x - x_{t,i})^2 + (y - y_{t,i})^2}{x_{r,i}^2 + y_{r,i}^2}} \right) \quad (8)$$

III. EVALUATION OF THE FIXED-POINT REPRESENTATION ON THE PROPOSED ALGORITHM

Considering the aforementioned processing, and in order to take advantage of the versatility of SoCs [17] [24], the proposed algorithm is divided into two groups: the Correlator/Demodulator, the Peak Detector, and the Impact Point blocks are implemented in hardware (PL, Programmable Logic), and the Positioning block is implemented in software (PS, Processing System). The hardware elements should be defined in a fixed-point representation, which can affect the final performance of the proposal. The purpose is to avoid or reduce quantization errors as much as possible, with a trade-off with the resource consumption.

The signal $r[n]$ acquired by an ADC (Analog Digital Converter) is initially assumed to have 12 bits (Q12.0, considering all of them as integers); it is demodulated with a square modulation symbol of $+1$ and -1 (Q2.0), with only additions and subtractions, resulting in a final quantization Q16.0, as shown in Fig. 7.

The demodulated signals $d[n]$ are sent into the correlation block, which is divided into two phases, as detailed in Section II-A. Since there is a one-bit increase for each level of the correlation architecture depicted in Fig. 5, the quantization increases to 23 bits (Q23.0) at the output of the efficient correlator for complementary sets (ESSC). Furthermore, as it is essential to collect the eight partial correlation signals computed by the two ESSCs, the final output of the complete efficient correlator for LS codes includes three bits more, resulting in a total quantization for each of the three correlation signals $C[n]$ of 26 bits (Q26.0).

As shown in Fig. 7, there is no change in the quantization in the maximum detection block. Only a comparison process is performed here to determine the maximum values of the correlation signals $C[n]$. The selected representation changes in the next stage of the proposed processing, as shown in Fig. 7, because the maximum correlation values, V_{sum}, V_{lr} and V_{bt}, previously determined, are normalized by the sum V_{sum}; this division results in fractional bits for the ratios P_x and P_y, with Q2.16. Due to the multiplications carried out in

the impact point calculation step, the quantization in the output signals (x_r, y_r) will rise two bits in the integer part and one bit in the fractional one, resulting in a final representation Q4.17. The input data for the positioning step comprises these impact points.

IV. SIMULATION RESULTS

The results presented hereinafter were obtained using a 2×2 m^2 simulated environment with a height of 3.4 m. The simulation is run with four QADA-type receivers, and one transmitter LED. As depicted in Fig. 1, the four receivers describe a parallelogram with a gap of 5 cm between them and their axes remain misaligned; this discards any geometric singularity that may impact the final position. The simulations are carried out with SNR=10 dB, obatined by adding a Gaussian noise in the electrical signals received by the QADA. Furthermore, the channel attenuation model is applied [10]. One thousand six hundred eighty-one test points were evaluated in simulations, with 20 realizations per each. These points are distributed along one of the QADA array's four quadrants, due the distribution's geometrical symmetry (in the rest of the quadrants, the behavior is similar).

Figure 8 shows these realizations for points considered in a horizontal projection; these results were obtained using the fixed-point representation described above. Note that points under the vertical of the QADA array have lower dispersion in the X and Y-axes in the position estimation than points further away. Figures 9, 10, and 11 show the Position Dilution of Precision (PDOP), Horizontal Dilution of Precision (HDOP), and Verical Dilution of Precision (VDOP) of the estimated results, respectively. Those are obtained by calculating the square root of the squares of the standard deviations of the estimates of the results obtained, as detailed in (9); where σ_x^2, σ_y^2, and σ_z^2 represent the square of the standard deviation for the x, y, and z coordinates, respectively, and σ_0 is the standard deviation of the adding noise (mean $\bar{x} = 1$, standard deviation $\sigma = 0.0001$). The results indicate that there are no locations with singularities and that, as predicted, estimates get more accurate as you get closer to the center of the coverage region.

Figure 8 represents the dispersion variation in the X and Y axes for all the simulated points. It can be observed that the estimates closer to the center of the QADA array have a lower dispersion than those located farther away. Only one quadrant is shown since, by symmetry, the other three have the same distribution. The dispersion on the Z-axis is more remarkable because it accumulates the inaccuracies

resulting from the (x,y) coordinates calculation. Table I shows the mean absolute errors and standard deviations for all the evaluated points. Finally, Fig. 12 shows the absolute errors in position estimation for each axis as a global CDF (Cumulative Distribution Function).

$$PDOP = \frac{\sqrt{\sigma_x^2 + \sigma_y^2 + \sigma_z^2}}{\sigma_0}$$

$$HDOP = \frac{\sqrt{\sigma_x^2 + \sigma_y^2}}{\sigma_0} \qquad (9)$$
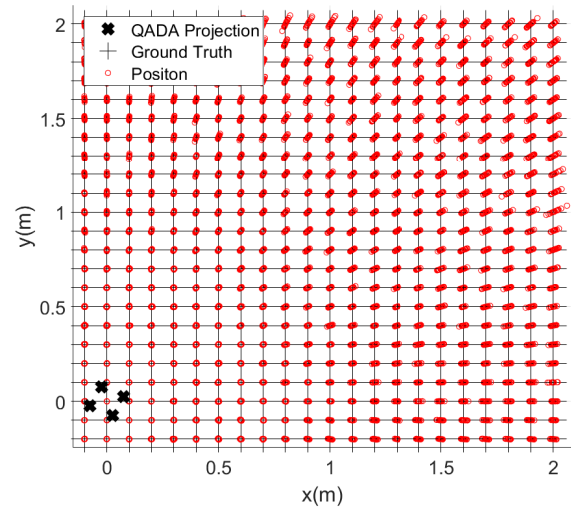
$$VDOP = \frac{\sqrt{\sigma_z^2}}{\sigma_0}$$

Fig. 8. Position estimates for all the points considered in simulation.

V. CONCLUSIONS

An indoor 3D infrared location system based on four-quadrant photoreceptors and a transmitting LED has been described in this work. The proposal details the hardware architecture of the QADA detector's processing and the fixed-point representation coming from a FPGA-based implementation on the estimation of the LED emitter's position. Simulations in a scenario with a dimension of 2×2 m^2 and a height of 3.4 m have been performed to verify the study, with mean absolute positioning errors of 0.0039 m, 0.0040 m, and 0.0131 m in the coordinates x, y, and z, respectively. Similarly, the standard deviations are 0.0034 m, 0.0035 m, and 0.0111 m.
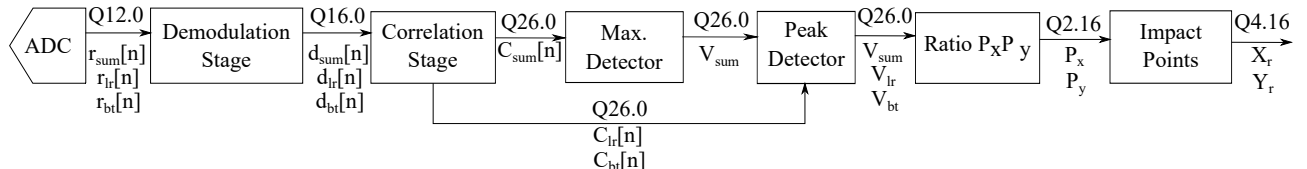

Fig. 7. Fixed-point representation selected for the demodulation/correlation stage.
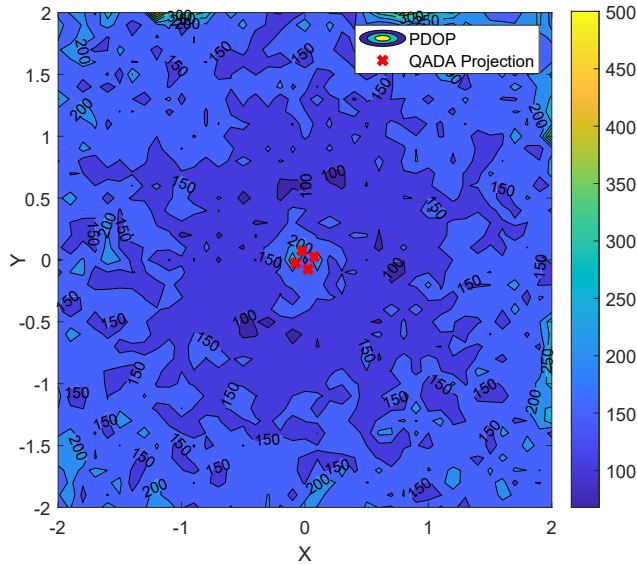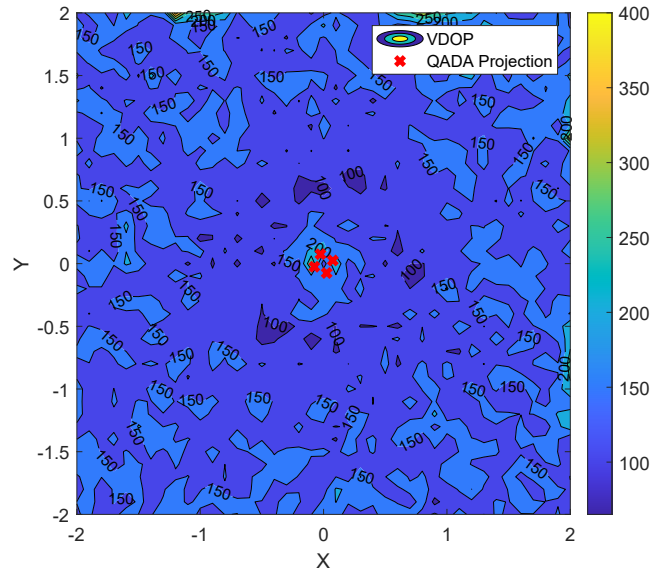
Fig. 9. PDOP estimation for the simulated environment.

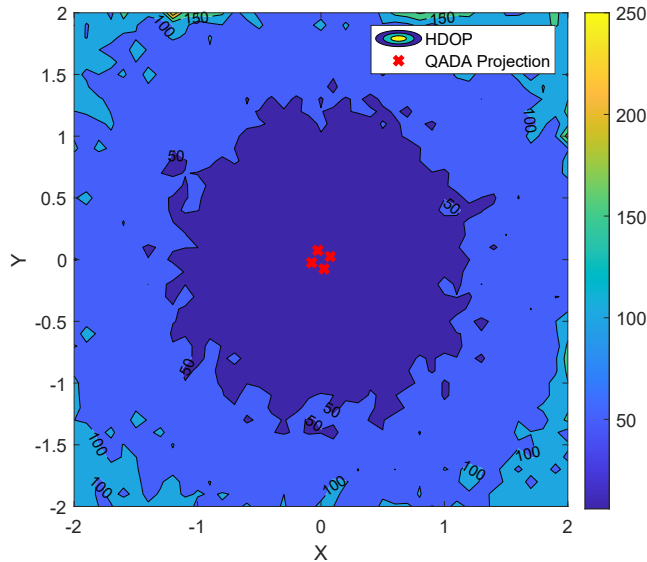Fig. 11. VDOP estimation for the simulated environment.

Fig. 10. HDOP estimation for the simulated environment.

Fig. 12. Absolute error CDF for every point studied in the simulation.

REFERENCES

[1] J. Ureña, *et al.*, "Acoustic local positioning with encoded emission beacons", *Proc. IEEE*, vol. 106, no. 6, pp. 1042-1062, J un. 2018.

[2] C. Wang, L. Wang, X. Chi, S. Liu, W. Shi, and J. Deng, "The research of indoor positioning based on visible light communication", *China Communications*, vol. 12, no. 8, pp. 85-92, 2015.

[3] T. H. Do, M. Yoo, "Performance Analysis of Visible Light Communication Using CMOS Sensors", *Sensors*, vol. 16(3), no. 309, pp. 1-23, 2016.

[4] T. H. Do, M. Yoo, "Potentialities and challenges of VLC based outdoor positioning", *International Conference on Information Networking (ICOIN)*, pp. 474-477, 2015.

[5] N. Rajagopal, P. Lazik, A. Rowe, "Visual light landmarks for mobile devices", *roceedings of the 13th International Symposiumon Information Processing in Sensor Networks*P, pp. 249–260, 2014.

[6] C. Danakis, M. Afgani, G. Povey, I. Underwood, H. Haas, "Using a CMOS camera sensor for visible light communication",*Proceedings of the Globecom Workshops (GC Wkshps)* , pp. 1244–1248, 2012.

[7] P. H. Pathak, X. Feng, P. Hu, P. Mohapatra, "Visible Light Communication, Networking, and Sensing: A Survey, Potential and Challenges," *IEEE Communications Surveys & Tutorials*, vol. 17(4), pp. 2047-2077, 2015.

[8] Y. Cai, W. Guan, Y. Wu, C. Xie, Y. Chen, L. Fang, "Indoor High Precision Three- Dimensional Positioning System Based on Visible Light Communication Using Particle Swarm Optimization", *IEEE Photonics Journal*, vol. 9(6), pp. 1-20, 2017.

[9] T. Q. Wang, Y. A. Sekercioglu, A. Neild, J. Armstrong, "Position Accuracy of Time-of-Arrival Based Ranging Using Visible Light With Application in Indoor Localization Systems", *Journal of Lightwave Technology*, vol. 31(20), pp. 3302-3308, 2013.

[10] S. Cincotta, C. He, A. Neild, J. Armstrong, "High angular resolution visible light positioning using a quadrant photodiode angular diversity aperture receiver (QADA)", *Optics Express*, vol. 26(7), pp. 9230-9242, 2018.

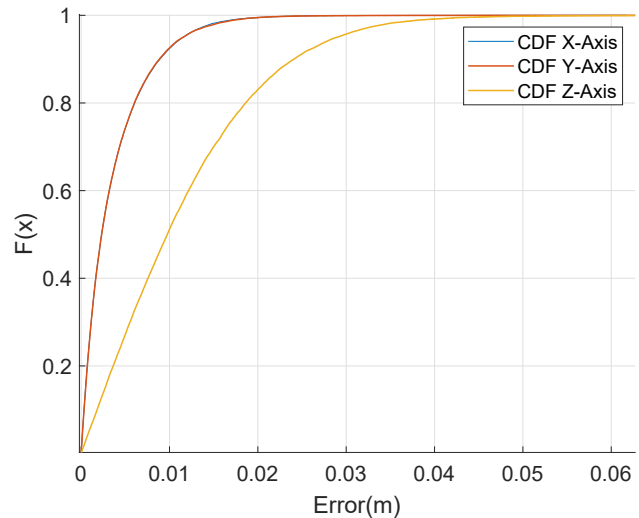[11] S. H. Yang, H. S. Kim, Y. H. Son, S. K Han, "Three-Dimensional

TABLE I
MEAN ABSOLUTE ERROR AND STANDARD DEVIATION.

	Mean absolute error			standard deviation		
	X (m)	Y (m)	Z (m)	X (m)	Y (m)	Z (m)
Total	0.0039	0.0040	0.0131	0.0034	0.0035	0.0111

Visible Light Indoor Localization Using AOA and RSS With Multiple Optical Receivers", *Journal of Lightwave Technology*, vol. 32(14), pp. 2480-2485, 2014.

[12] E. Gonendik, S. Gezici, "Fundamental Limits on RSS Based Range Estimation in Visible Light Positioning Systems", *IEEE Communications Letters*, vol. 19(12), pp. 2138-2141, 2015.

[13] H. Steendam, T. Q. Wang, J. Armstrong, "Theoretical Lower Bound for Indoor Visible Light Positioning Using Received Signal Strength Measurements and an Aperture-Based Receiver", *Journal of Lightwave Technology*, vol. 35(2), pp. 309-319, 2017.

[14] C. Wang, L. Wang, X. Chi, S. Liu, W. Shi, J. Deng, "The research of indoor positioning based on visible light communication", *China Communications*, vol. 12(8), pp. 85-92, 2015.

[15] C. Xie, W. Guan, Y. Wu, L. Fang, Y. Cai, "The LED-ID Detection and Recognition Method Based on Visible Light Positioning Using Proximity Method", *IEEE Photonics Journal*, vol. 10(2), pp. 1-16, 2018.

[16] T-H. Do, M. Yoo, "An in-Depth Survey of Visible Light Communication Based Positioning Systems", *Sensors 16(5)*, no. 678, pp 1-40, 2016.

[17] S. Knapp, "Field configurable system on chip devices architecture", *Proc. of the 22nd IEEE Custom Integrated Circuits Conference (CICC)*, pp. 155-158, 2000.

[18] E. Aparicio-Esteve, Á. Hernández, J. Ureña; "Design, Calibration, and Evaluation of a Long-Range 3-D Infrared PositioningSystem Based on Encoding Techniques", *IEEE Trans. Instrum. Meas.*, 70, 1–13, 2020.

[19] M. C. Pérez. "Generación y correlación eficiente de códigos binarios derivados de conjuntos de secuencias complementarias para sistemas ultrasónicos". Tesis doctoral, Departamento de Electrónica, Universidad de Alcalá, Alcalá de Henares, España, 2009.

[20] E. Aparicio-Esteve, Á. Hernández and J. Ureña, "Evaluation of MAI Effect in Encoding Techniques for an Infrared Positioning System," 2020 IEEE International Instrumentation and Measurement Technology Conference (I2MTC), 2020, pp. 1-6.

[21] IEEE 1789-2015 IEEE Recommended Practices for Modulating Current in High-Brightness LEDs for Mitigating Health Risks to Viewers, IEEE Standards Association, June 2015

[22] S. Z. Budisin "Efficient pulse compressor for Golay complementary sequence", *IEEE Electronics Letters*, 27(3):2019-220, 1991.

[23] B. M Popovic. "Efficient Golay correlator", *IEEE Electronics Letters*, 35(17):1427-1428, 1999.

[24] J. Becker, N. Libeau, T. Pionteck, M. Glesner, "Efficient mapping of presynthesized IP-cores onto dynamically reconfigurable array architectures", *Proc of the 11th International Conference on Field-Programmable Logic and Applicacions (FPL)*, pp. 584-589, 2001.